Dalton Transactions

PAPER

View Article Online
View Journal | View Issue

Cite this: *Dalton Trans.*, 2015, **44**, 8419

Formylated chloro-bridged iridium(III) dimers as OLED materials: opening up new possibilities†

Michael Y. Wong,[a] Guohua Xie,[b] Clarisse Tourbillon,‡[c] Martina Sandroni,§[c] David B. Cordes,[a] Alexandra M. Z. Slawin,[a] Ifor D. W. Samuel[b] and Eli Zysman-Colman*[a]

Received 10th October 2014,
Accepted 8th January 2015

DOI: 10.1039/c4dt03127j

www.rsc.org/dalton

In this study, a series of four formyl-substituted chloro-bridged iridium(III) dimers were prepared. Their absorption, photophysical and electrochemical properties were studied in dichloromethane solution. It was found that as the formyl content increased on the cyclometalating ligands, emission unexpectedly became brighter. Organic light-emitting diodes (OLEDs) were fabricated using each of these iridium dimers as the emitter. The OLED fabricated using the brightest of the series, **2b**, as the dopant afforded a decent external quantum efficiency (EQE) of 2.6%. This suggests that chloro-bridged iridium dimers are potential candidates as solid-state emitters.

Introduction

Neutral mononuclear cyclometalated iridium complexes have received intense attention as emitters for organic light emitting diodes (OLEDs) in lighting and visual displays.[1] Their privileged use is due to the phosphorescent nature of the emission, which is mediated by the iridium metal that facilitates intersystem crossing due to spin–orbit coupling.[2] Thus, unlike OLED devices based on fluorescent emitters whose internal quantum efficiencies (IQE) are capped by 25% according to spin statistics, 100% of the excitons can be harvested in phosphorescent electroluminescent devices.[3] Additionally, iridium(III) complexes typically exhibit bright emission at room temperature that can be tuned across the visible spectrum as a function of substitution about and combination of ligands, possess short radiative lifetimes that mitigates undesirable triplet–triplet annihilation and are thermally and chemically stable.[4]

The majority of syntheses of these mononuclear iridium complexes proceeds *via* the formation of a dichloro-bridged iridium intermediate of the form $[Ir(C\hat{}N)_2Cl]_2$ where C^N is a cyclometalating ligand such as the commonly used 2-phenylpyridinato, ppy. Despite the thousands of articles relating to the photophysical study of mononuclear iridium complexes, since the seminal work by Watts and co-workers[5] almost thirty years ago, the study of these iridium dimers has often been overlooked.[6] This has certainly been influenced by the fact that the parent iridium dimer, $[Ir(ppy)_2Cl]_2$, and indeed most dimers in this family, are very poorly emissive[5b,7] in toluene solution while *fac*-$Ir(ppy)_3$, under similar conditions, exhibits a photoluminescence quantum yield, Φ_{PL}, ranging from 70% to near unity, depending upon the medium.[8] Bryce, Monkman and co-workers[6b] recently reported the first examples of dichloro-bridged iridium complexes used as emissive dopants in OLEDs. Employing complexes with substituted fluorenylpyridine C^N ligands dispersed in a PVK host polymer, they could obtain OLEDs with EQEs ranging from 0.6 to 4% and power efficiencies of 0.4–3.53 lm W^{-1}.

Monoformyl-substituted C^N ligands incorporated onto mononuclear iridium complexes have been investigated,[9] particularly by Lo and co-workers[10] as a tool for grafting on receptor units for bioimaging. To the best of our knowledge, no one has explored the optoelectronic properties of the dichloro-bridged dinuclear complexes bearing formyl-substituted ppy ligands. In this study, we synthesized and characterized a series of dichloro-bridged iridium dimers whose structures are shown in Chart 1. The optoelectronic properties of **1a–2b** were probed as a function of the regiochemistry and number of formyl units present on the cyclometalating (C^N) ligands. Unexpectedly, when the number of formyl units increased, the

[a]*Organic Semiconductor Centre, EaStCHEM School of Chemistry, University of St Andrews, St Andrews, Fife KY16 9ST, UK.*
E-mail: eli.zysman-colman@st-andrews.ac.uk;
http://www.zysman-colman.com; Fax: +44 (0)1334 463808; Tel: +44 (0)1334 463826
[b]*Organic Semiconductor Centre, School of Physics and Astronomy, University of St. Andrews, North Haugh, St. Andrews, Fife KY16 9SS, UK*
[c]*Département de Chimie, Université de Sherbrooke, Sherbrooke, Québec, Canada J1 K 2R1*

† Electronic supplementary information (ESI) available. CCDC 1026256–1026259. For ESI and crystallographic data in CIF or other electronic format see DOI: 10.1039/c4dt03127j

‡ Current address: Laboratoire PPSM - CNRS UMR 8531, ENS Cachan, 61 Av du Président Wilson, 94235 Cachan Cedex France.

§ Current address: CEMCA UMR CNRS 6521, Université de Bretagne Occidentale, 6 av. Victor Le Gorgeu, Brest, France, 29200.

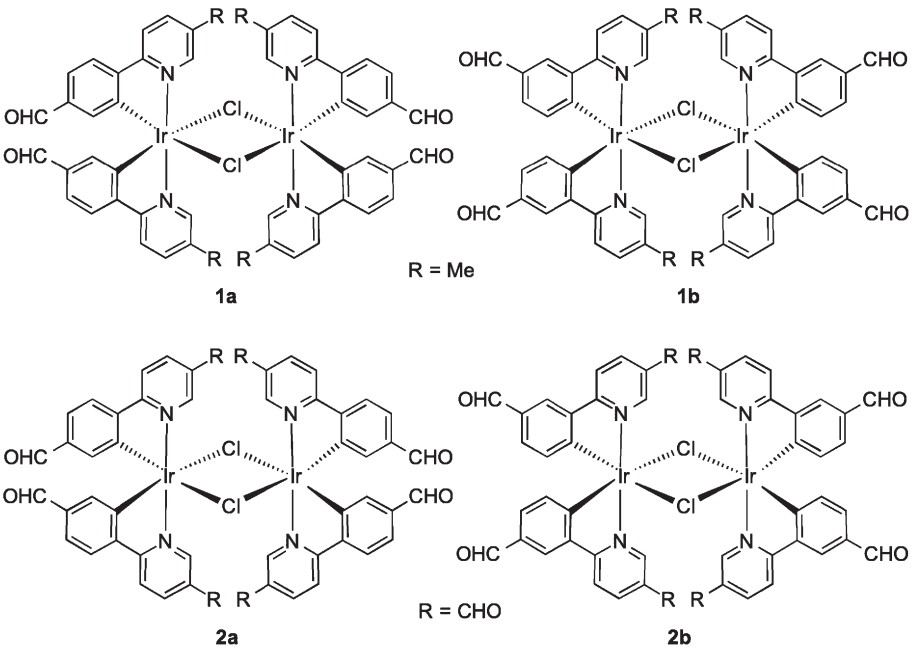

Chart 1 Chemical structures of the complexes presented in this study.

Φ_{PL} of the complex increased significantly, with **2a** the brightest at 15.7% in DCM. OLED devices were fabricated using these complexes as phosphorescent dopants with performances modestly reduced in comparison to those reported by Bryce, Monkman and co-workes.[6b] This study corroborates their earlier report that dichloro-bridged dinuclear iridium complexes, even those simply functionalized as is the case here, can be used as the emissive layer in viable OLED devices.

Results and discussion

Ligand and complex synthesis

The formyl-substituted cyclometalating (C^N) ligands were obtained in excellent yields (86–92%) following a Suzuki–Miyaura[11] coupling between the suitably formylated arylboronic acid and either 2-bromo-5-methylpyridine or 2-bromo-5-formylpyridine (Scheme 1). The use of $Pd(PPh_3)_4$ as the catalyst resulted in much cleaner conversion to product than with $Pd(PPh_3)_2Cl_2$, wherein significant homocoupling of the arylboronic acid was observed. The latter functionalized pyridine was itself obtained in 63% yield *via* regioselective lithium halide exchange in diethyl ether, quench with DMF and subsequent hydrolysis.[12]

The dichloro-bridged iridium(III) dimers were prepared according to the protocol first reported by Nonoyama.[13] While **1a** and **1b** were obtained in 58 and 61%, respectively and were analytically pure following precipitation from a refluxing 3 : 1 v/v mixture of 2-ethoxyethanol–water, under these same conditions the synthesis of **2a** and **2b** resulted in very complicated

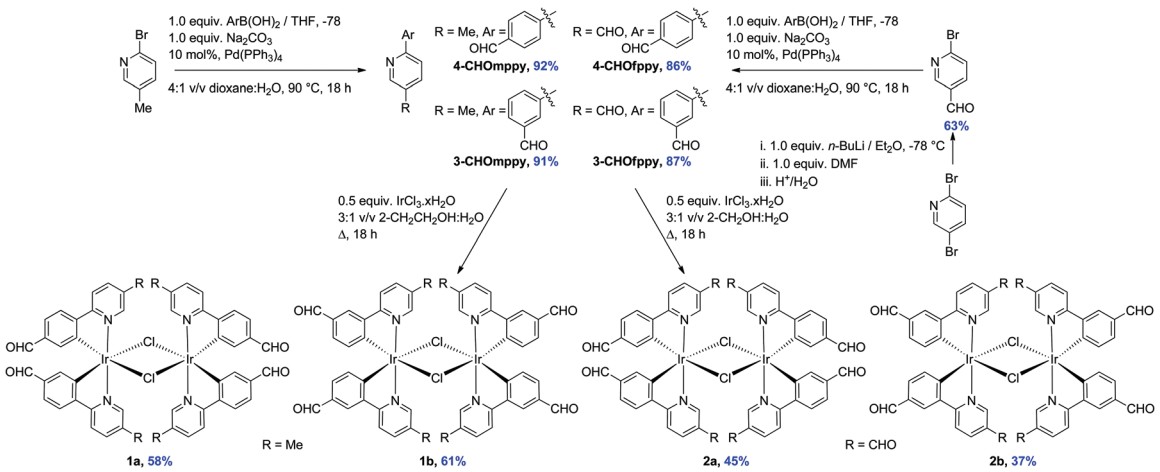

Scheme 1 Synthesis of formyl-substituted C^N ligands and iridium dimer complexes **1a–2b**.

^{1}H NMR spectra. However, when the synthesis was repeated in a refluxing 3 : 1 v/v mixture of 2-methoxyethanol–water, **2a** and **2b** precipitated from the solution and could be obtained in more modest 45 and 37% yields, respectively. Complexes **1a–2b** were characterized by ^{1}H NMR, ^{13}C NMR, Mp, EA and HRMS. Additionally single crystals of sufficient quality for X-ray diffraction analyses for all four complexes were obtained (*vide infra*).

Solution state characterization

Fig. 1 shows the aromatic region of the ^{1}H NMR spectra for **1a** and **4-CHOmppy** (for corresponding comparison of ^{1}H NMR for **1b**, **2a** and **2b** with their respective C^N ligands see Fig. S19–S22, ESI†). Eight well-resolved resonances are observed in the ^{1}H NMR of **1a** in $CDCl_3$, the result of chemical non-equivalence of the H_{3A}/H_{5A} protons upon cyclometalation. Structural assignments are based on 2D-COSY NMR experiments and a comparison of our 1D NMR data with those previously reported by Watts and co-workers, and more recently Schubert and co-workers.[5c,14] The resonance for H_{A5} at δ 6.16 is significantly shifted upfield due to the formal anionic charge of the cyclometalating phenyl ring.[5a,15] By contrast, H_{B6} is shifted downfield at δ 9.07 upon complexation.[5c] The regiochemistry of cyclometalation in **1b** and **2b** can be simply determined from the presence of H_{A2}, which has a characteristic chemical shift at *ca.* δ 6 and a coupling constant of *ca.* 8 Hz. Thus, the formyl groups on the phenyl ring in these two complexes are located exclusively *para* to the iridium metal. The pattern of signals in the ^{1}H NMR and the presence of only thirteen ^{13}C NMR resonances also points to a single configuration coordination mode for the four complexes, with the arrangement of the nitrogen atoms of the pyridine moieties *trans* with respect to each other, as is typical under the reaction conditions. Though the synthesis is not stereoselective and statistical mixtures of ΔΔ, ΛΛ and ΔΛ diastereomers should exist in solution, by ^{1}H NMR only a single set of resonances exists. Single crystal X-ray diffraction results reveal only the presence of only a racemic mixture of ΔΔ and ΛΛ isomers. (*vide infra*).

The MALDI HRMS show low intensity molecular ions for all four complexes. In all four mass spectra, a fragmentation peak with a mass-to-charge ratio (*m*/*z*) half that of the molecular ion is always observed, which resulted from homo-cleavage of the molecular ion under MS conditions. Similar observations have been reported in the literature.[16]

Solid-state characterization

All crystals were grown by vapour diffusion of diethyl ether into saturated DCM solution of the complexes. The connectivity of bonds provides an absolute proof of structure. All four complexes adopt similar dinuclear structures (Fig. 2) with compounds **1a**, **1b**, and **2b** crystallising in the monoclinic space group $P2_1/c$, in unit cells of broadly similar sizes, and one molecule of complex in the asymmetric unit, while compound **2a** crystallises in the space group $P2_1/n$, but with a unit cell of close to twice the size, and two molecules of complex in the asymmetric unit. The complexes adopt a slightly distorted octahedral coordination environment about the iridium(III) centres, with Ir–N *trans* to each other and Ir–C *cis*, in common with other examples of $[Ir(C^N)_2Cl]_2$ complexes.[5c,6,15–17] While this arrangement can be readily deduced in the cases of complexes **1a**, **1b**, and **2b**, for complex **2a**, comparison of potential Ir–C/N distances, as well as the ^{1}H NMR data, confirm the *trans*-N arrangement. Bond parameters about the iridium(III) are unexceptional (Fig. 2), as are the Ir···Ir separations [3.7867(9) to 3.8068(19) Å]. In an analogous manner to related complexes, all four complexes display racemic ΔΔ and ΛΛ diastereomers, rather than the *meso* ΔΛ form. All four structures

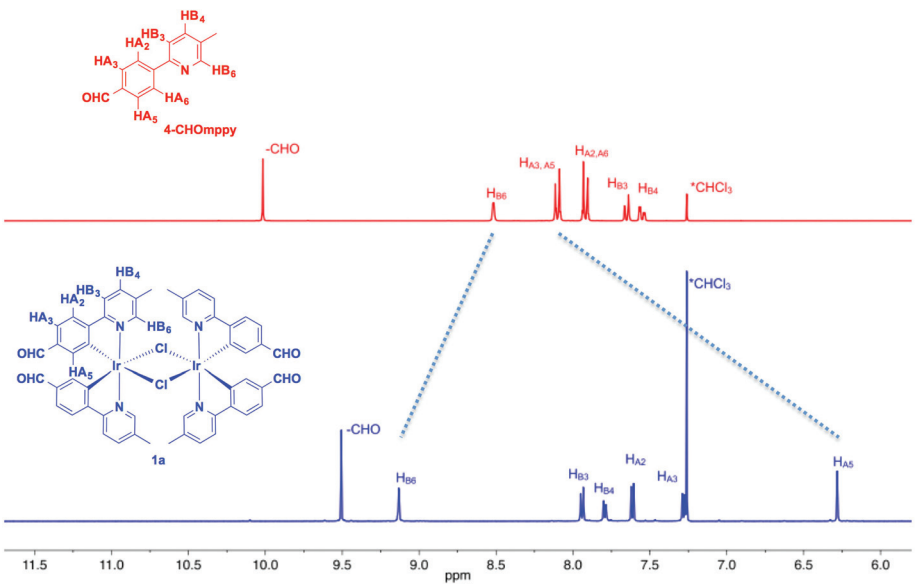

Fig. 1 Stacked ^{1}H NMR spectra of aromatic region **4-CHOmppy** (red) and complex **1a** in $CDCl_3$ at 298 K.

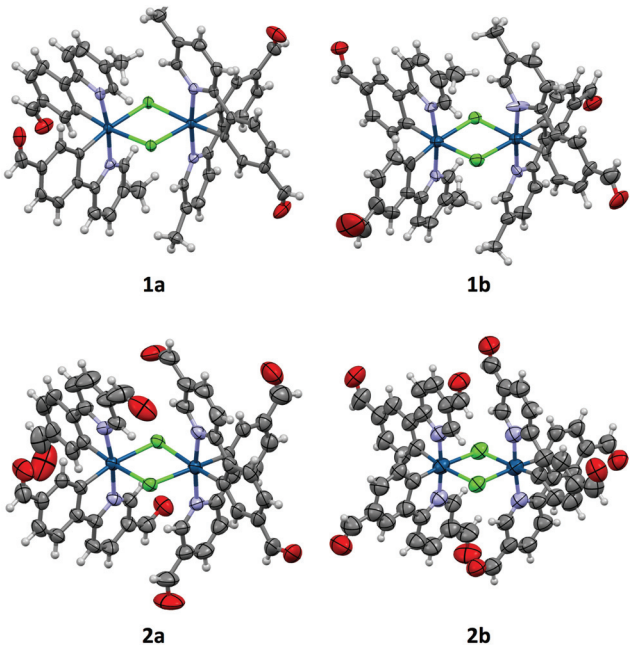

Fig. 2 Crystal structures of complexes **1a–2b**, with solvent molecules omitted. Thermal ellipsoids are drawn at the 50% probability level for **1a**, **1b**, and **2a**, and at the 30% probability level for **2b**. Bond lengths in Å: **1a** Ir–C [1.989(9)–2.00(1)]; Ir–N [2.035(7)–2.059(7)]; Ir–Cl [2.494(2)–2.529(2)]; **1b** Ir–C [1.99(2)–2.04(2)]; Ir–N [2.01(2)–2.06(2)]; Ir–Cl [2.498(6)–2.536(6)]; **2a** Ir–C [1.988(6)–2.023(7)]; Ir–N [2.035(5)–2.058(5)]; Ir–Cl [2.510(2)–2.527(2)]; **2b** Ir–C [1.87(2)–1.92(2)]; Ir–N [1.95(2)–2.00(2)]; Ir–Cl [2.491(7)–2.542(6)]. Bond angles in degrees: **1a** N–Ir–C [80.2(3)–81.2(3)] Cl–Ir–Cl [81.34(7)–81.43(7)]; **1b** N–Ir–C [81.5(2)–83.1(8)] Cl–Ir–Cl [81.5(2)–81.6(2)]; **2a** N–Ir–C [79.9(2)–80.8(2)] Cl–Ir–Cl [81.83(5)–82.13(5)]; **2b** N–Ir–C [80.8(9)–83.1(9)] Cl–Ir–Cl [81.4(2)–82.2(2)].

showed space open to solvent within them. In **1a** and **2a** this could be modelled as either one (disordered) or two molecules of CH_2Cl_2 per complex, respectively, with no void space remaining. In **1b** and **2b** however, no solvent molecules could be sensibly modelled, resulting in large void spaces. In **1b**, these run along the *a*-axis whereas in **2b**, channels are narrow and do not run straight along a single axis; additional thin void spaces can be seen in the *ac*-plane.

Various interactions are seen to be common to the four complexes, both intramolecular, for maintaining the molecular geometries seen, and intermolecular, for providing stabilising interactions between molecules. Intermolecular interactions can be seen as weak C–H···Cl hydrogen bonds that are present between the CH(α) adjacent to the nitrogen atom of the pyridyl rings of the C^N ligands and the bridging chlorides of the complexes [H···Cl distances ranging from 2.50 to 2.70 Å, with C···Cl separations of 3.311(8) to 3.35(2) Å]. These hydrogen bonds are complemented, in all cases except **2b**, by C–H···π interactions between a proximal CH of a phenyl ring, and the π-system of the pyridyl of an adjacent ligand; H···centroid distances ranging from 2.93 to 2.94 Å, with C···centroid separations of 3.72(3) to 3.725(7) Å (Fig. 3).

Common intermolecular interactions in the complexes include both interactions between the complexes and solvent,

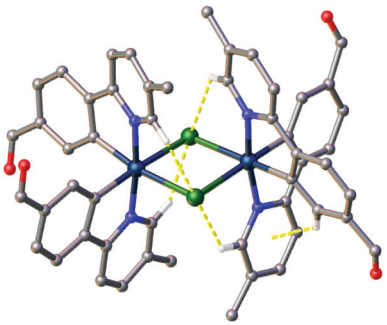

Fig. 3 View of complex **1a** showing the intramolecular interactions present in the complexes. Interactions shown as dashed yellow lines, hydrogen atoms not involved in the interactions were omitted.

for those where the solvent could be resolved within the structure, and between adjacent complex molecules. Complex-to-solvent interactions consist of both C–H···π and weak C–H···Cl hydrogen bonds, the latter involving aryl hydrogens. Interactions between complexes follow a similar pattern. A few C–H···π interactions are observed, although at sufficient interatomic distances [H···centroid 2.73–2.93 Å, C···centroid 3.650(7)–3.874(10) Å] to be relatively unimportant if taken by themselves. They are reinforced, however, by sets of weak C–H···O hydrogen bonds, involving both aryl and (where they exist as in **1a** and **1b**) alkyl hydrogens, at H···O distances of 2.19 to 2.59 Å, and C···O separations of 2.999(15) to 3.542(13) Å.

As well as these sets of conserved interactions, there are some intermolecular interactions that occur in some, but not all, of these complexes. Complexes **1a**, **1b**, and **2b** show further interaction involving their bridging chlorides. These are C–H···Cl hydrogen bonds involve the formyl protons of adjacent complexes. The H···Cl distances range from 2.51 to 2.82 Å, with corresponding C···O separations of 3.32(4) to 3.70(3) Å. An additional feature of the interactions in these three complexes is that none of them show π···π interactions (no centroid···centroid distances of less than 3.91 Å is present). Complex **2a**, on the other hand shows quite different interactions to these (Fig. 4). The first of these is a π-stacking

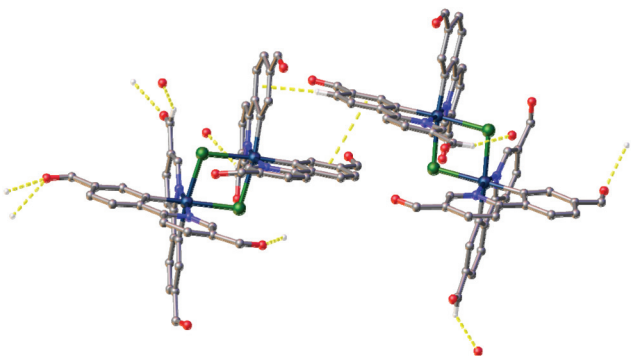

Fig. 4 View of complex **2a** showing the intermolecular interactions observed in this complex but not the others. Interactions shown as dashed yellow lines, hydrogen atoms not involved in the interactions were omitted.

interaction between proximal phenyl rings of the two molecules in the asymmetric unit. The centroid···centroid distance is 3.767(4) Å, with an inclination between ring-planes of 0.2(4)°. This interaction is reinforced by one of the C–H···π interactions mentioned earlier, between a hydrogen on one of the π-stacking rings, and another ring centroid on the adjacent complex. The second set of different interactions concerns weak hydrogen bonds involving the formyl protons. Unlike in the other three complexes, in **2a** these do not interact with the bridging chloride atoms, but form an extensive network of C–H···O interactions with other formyl groups (Fig. 4). The H···O distances in these interactions vary between 2.30 and 2.52 Å, with C···O separations of 3.102(14) to 3.346(13) Å. From the interatomic distances in these interactions it may be deduced that the molecules of complex in **2a** are held together more tightly in the solid state, and interact more strongly than those in the other complexes.

Electrochemical properties

The electrochemical properties of **1a–2b** were studied in nitrogen-saturated DCM at room temperature using nNBu$_4$PF$_6$ as the supporting electrolyte and using Fc/Fc$^+$ as an internal standard. All potentials are referenced to SCE (Fc/Fc$^+$ = 0.46 V in DCM).[18] The results are compiled in Table 1 while CV traces are shown in Fig. 5. The CV behavior was reproducible across a range of scan rates ranging from 50 to 1000 mV s^{-1} though at higher scan rates the redox waves broadened, rendering analysis more difficult. All complexes in this study showed essentially quasi-irreversible or irreversible electrochemistry as $i_{pa}/i_{pc} \ll 1$.

The parent dimer [Ir(ppy)$_2$Cl]$_2$ shows two one-electron oxidation waves at 1.00 and 1.26 V indicating that there is electronic communication between the two iridium centres mediated by the chloride bridges. The oxidations are assigned to the Ir^{III}/Ir^{IV} redox couple with significant contribution from the aryl ring. No reduction is observed within the solvent window. This profile matches that originally reported by Watts and co-workers.[5b] The introduction of an electron-withdrawing formyl group onto the phenyl moiety of the C^N ligand in **1a** and **1b** results in an expected shift to more positive potential of both oxidation waves, corresponding to a stabilization of the HOMO on each of the two iridium centers. Placement of the formyl group *para* to the Ir–C bonding results in a 100 mV anodic shift of both oxidation waves in **1b** compared to **1a**. The additional of a second formyl group at the 5-position of the pyridine fragment of the C^N ligands makes the first oxidation more difficult by 0.21 and 0.23 V for **2a** and **2b** *versus* **1a** and **1b**, respectively.

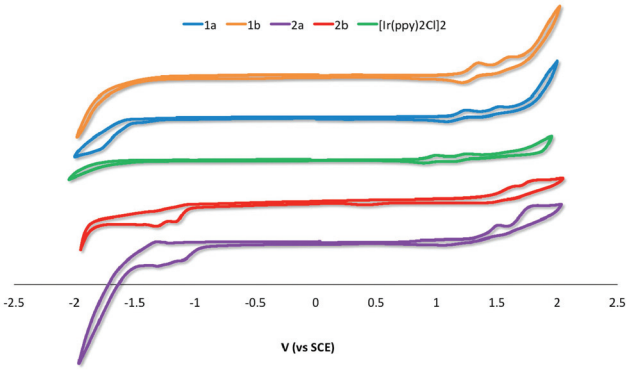

Fig. 5 CV traces for **1a–2b** and [Ir(ppy)$_2$Cl]$_2$ recorded at 298 K at 50 mV s^{-1} in deaerated DCM with 0.1 M (nBu$_4$N)PF$_6$.

For **1a** and **1b** no reduction waves are observed. However, for **2a** and **2b** two irreversible reduction waves are now observed pointing to a LUMO involving the 5-formyl group. The LUMO is stabilized by a further 60 mV in **2a** compared to **2b**; the second reduction in both of these complexes occurs at *ca.* −1.31 V.

The band gaps ΔE for **2a** and **2b** were determined from the electrochemical data and are 2.56 and 2.74 eV, respectively. The band gaps for **1a** and **1b** at 2.38 and 2.58 eV, respectively, were extrapolated from the tailing edge at 10% intensity of the lowest energy absorption band, corresponding to the energy of the 0,0 transition. This method certainly underestimates this parameter by at least 0.65 eV as the HOMO to LUMO transition does not account for the binding energy associated with ionization.[20]

UV-visible absorption spectroscopy

The UV-visible absorption spectra for **1a–2b** and [Ir(ppy)$_2$Cl]$_2$ were recorded in aerated DCM at 298 K and are shown in Fig. 6. The results are summarized in Table S1.†

Table 1 Electrochemical data of **1a–2b** and [Ir(ppy)$_2$Cl]$_2$ [a,b]

Complex	$E^{ox}_{pa,1}$/V	$E^{ox}_{pa,2}$/V	$E^{red}_{pc,1}$/V	$E^{red}_{pc,2}$/V	ΔE_{redox}/V	E_{HOMO}/eV	E_{LUMO}/eV	ΔE/eV
[Ir(ppy)$_2$Cl]$_2$	1.00	1.26				−5.34	−2.85	2.49
1a	1.25	1.51				−5.59	−3.21[c]	2.38
1b	1.35	1.61				−5.69	−3.11[c]	2.58
2a	1.46	1.67	−1.10	−1.30	2.56	−5.80	−3.24	2.56
2b	1.58	1.72	−1.16	−1.31	2.74	−5.92	−3.18	2.74

[a] Conditions: CV traces recorded in N$_2$-saturated DCM solution with complex concentration at 10^{-4} M with 0.1 M nBu$_4$NPF$_6$ at 298 K; platinum wires were used as the working and counter electrodes, respectively while an Ag/AgCl reference electrode was employed; scan rate: 50 mV s^{-1}. Values are in V *vs.* SCE (Fc/Fc$^+$ *vs.* SCE = 0.46 V).[18] $\Delta E = -(E_{HOMO} - E_{LUMO})$; E_{pa} = anodic peak potential and E_{pc} = cathodic peak potential. [b] The HOMO and LUMO energies were calculated using the relation $E_{HOMO/LUMO} = -(E^{ox}_{pa,1}/E^{red}_{pc,1} + 4.8)$ eV, where $E^{ox}_{pa,1}/E^{red}_{pc,1}$ are the first oxidation or reduction peaks with respect to $E_{1/2}$ of ferrocene/ferrocenium redox couple.[19] [c] E_{LUMO} was estimated from optical band gap, $E_{0,0}$ determined from the low energy tail at 10% intensity of the lowest energy absorption band.

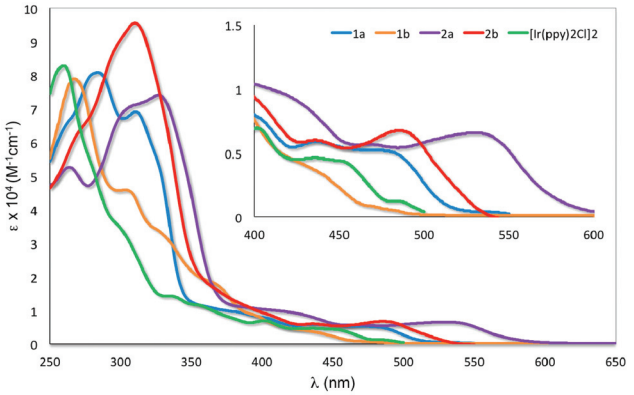

Fig. 6 UV-visible absorption spectra of **1a–2b** and $[Ir(ppy)_2Cl]_2$ in DCM at 298 K. Inset: zoomed UV-visible spectra for the region between 400–600 nm.

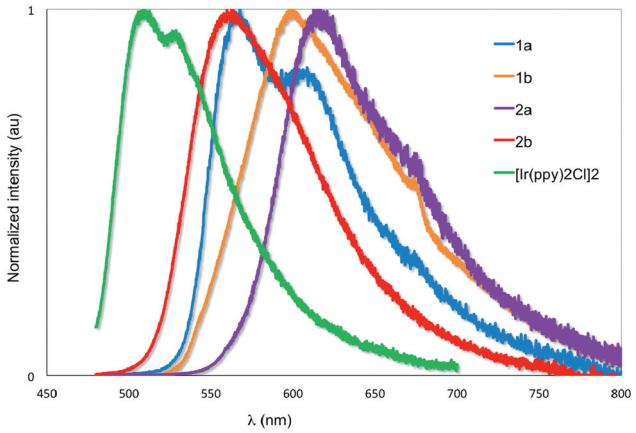

Fig. 7 Normalized emission spectra of **1a–2b** and $[Ir(ppy)_2Cl]_2$ in de-aerated DCM at 298 K. λ_{exc}: 455 nm.

All the iridium dimers possess intense absorption bands below *ca.* 350 nm corresponding to spin-allowed singlet ligand-centered (^{1}LC) $^1\pi$–π^* transitions.[6a] At lower energies, the absorption spectra are dominated by spin-allowed metal-to-ligand charge transfer (^{1}MLCT) and intraligand charge transfer (^{1}ILCT) transitions;[5a,b,18] spin forbidden ^{3}MLCT transitions are certainly also present at low energies due to the large spin–orbit coupling mediated by Ir. Similar to other homodinuclear iridium complexes,[21] the molar absorptivities of these complexes are approximately double than those of neutral mononuclear iridium complexes such as $[Ir(ppy)_2(pic)]$ (pic = picolinate).[22]

The absorption profile for **1a** and **1b** are similar, with **1a** being bathochromically shifted compared to **1b** and $[Ir(ppy)_2Cl]_2$. This red-shift in **1a** is caused by the electron-withdrawing 4-formyl group, which results in a stabilisation of both the occupied π and the unoccupied π* orbital of the C^N ligands and a smaller energy transition.[23] This red-shifting of the absorption spectrum is not observed in **1b**, with its HOMO–LUMO band blue-shifted compared to $[Ir(ppy)_2Cl]_2$. The change in regiochemistry of the formyl group on the phenyl fragment results in cross-conjugation with the pyridine moiety and a reduced influence on the energies of the anti-bonding orbitals. Additionally, the HOMO stabilising character of the 3-formyl group is more pronounced, as it is now *para* to the Ir–C bond. Similarly, the absorption of **2a** is bathochromically shifted with respect to **2b**. The magnitude of this red-shift is unexpected, particularly given the similar ^{1}MLCT absorption maxima reported by Bryce, Monkman and co-workers for a series of fluorenyl-containing iridium dimer complexes bearing 5-fluoro- or 5-methoxy-substituted pyridine moieties on the C^N ligands.[6b] The greater red-shifting of the absorption spectra for **2a** and **2b** compared to **1a** and **1b** results from the presence of the second formyl group, which further stabilises the LUMO that contains significant electron density on the pyridine ring of the ligand.

Emission spectroscopy

The emission properties of the five complexes were studied in degassed DCM at 298 K with the spectra shown in Fig. 7 and the results summarized in Table 2. Their emission profiles are broad with the presence of either two well-defined emission bands or the presence of a low energy emission shoulder. The emission is assigned to a mixed ^{3}MLCT/^{3}LC transition.[6a] The very weak emission of $[Ir(ppy)_2Cl]_2$ at 520 nm reproduces that previously reported by Watts and co-workers.[5c] The introduction of formyl groups causes a red-shift in the emission compared to the benchmark iridium dimer. The regiochemistry and quantity of the formyl groups have a dramatic impact on the photophysical properties of these complexes. Surprisingly, in **1a** the addition of the 4-formyl unit causes a red-shift of 1468 cm^{-1} and an accompanying order of magnitude increase in Φ_{PL} to 2.5%. By contrast, incorporation of electron-withdrawing fluorine atoms onto the C^N ligands in both mononuclear neutral[24] and charged[25] complexes causes a blue-shift in the emission due to large stabilization of the HOMO. Positioning the formyl group *para* to the Ir–C in **1b** causes a further red-shift of 1095 cm^{-1} compared to **1a**. Emission in **1b** is so weak as to preclude accurate determination of Φ_{PL}. The introduction of a second formyl group in **2b** causes a blue-shift in the emission compared to **1b**. Most striking, the emission for **2a** is not similarly blue-shifted compared to **1a** but is red-shifted by 1395 cm^{-1} and is the brightest of the series of iridium dimers with a Φ_{PL} of 15.7%. Only recently reported

Table 2 Solution state photophysical data of **1a–2b** and $[Ir(ppy)_2Cl]_2$ [a]

Dimer complex	λ_{em} (nm)	Φ_{PL} [b] (%)	τ_e [c] (ns)	k_r [d] ($\times 10^5$ s^{-1})	k_{nr} [e] ($\times 10^5$ s^{-1})
$[Ir(ppy)_2Cl]_2$	520	0.1	125	0.40	79.60
1a	563, 600	2.5	206	1.21	47.33
1b [f]	600	Emission too weak			
2a	611, 670(sh)	15.7	1980	0.79	4.26
2b	556	0.9	601	0.15	16.49

[a] Emission measured in N_2-saturated DCM at room temperature. [b] Relative to $Ru(bpy)_3(PF_6)_2$ (Φ_{PL} = 9.5% in degassed MeCN).[26] [c] λ_{exc}: 470 nm. [d] Calculated from $\Phi_{PL} = \tau_e \times k_r$. [e] Calculated from $\Phi = k_r/(k_r + k_{nr})$. [f] Emission too weak to determine Φ_{PL} or τ_e.

Table 3 Solid-state photophysical data of **1a–2b**

Dimer complex	λ_{PL} [a] (nm)	Φ_{PL} [b] (%)	Φ_{PL} [c] (%)
1a	562	1.0	10.3
1b[d]	—	—	—
2a	620	1.1	14.7
2b	555	2.6	35.6

[a] PL measurements of blended films of CBP : PBD : complexes (60 : 30 : 10 wt%) in a 60 nm thick film. [b] Φ_{PL} of neat films spin-coated onto a fused silica substrate from DCM solution. [c] Φ_{PL} of blended films of CBP : PBD : dimer complex (60 : 30 : 10 wt%) on a fused silica substrate. CBP is 4,4′-*N*,*N*′-dicarbazole-biphenyl and PBD is 2-(*tert*-butylphenyl)-5-biphenyl-1,3,4-oxadiazole. [d] Data not available due to weak emission.

fluorenyl annelated phenylpyridine C^N dichloro-bridged iridium dimers have shown brighter emission than **2a** for this class of complexes.[6b] Its emission lifetime, τ_e, is also an order of magnitude longer than the other complexes at nearly 2 μs. The primary reason for this enhanced emission is due to the large decrease in the non-radiative rate constant, k_{nr} caused by increased rigidity conferred by the more extensive hydrogen bonding interactions (*vide supra*).

In order to better understand the photophysics of the materials and their potential for OLEDs, the photoluminescence quantum yield of the solid films was measured. Neat films were studied and compared with films in which the test complex was blended with charge transporting materials. The latter films are generally preferable for OLEDs because diluting the chromophore usually reduces concentration quenching, and because the host materials can facilitate charge transport. The films were prepared by spin-coating the materials from DCM solution onto fused silica substrates, and the results are shown in Table 3. As with solution-state measurements, **1b** has minimal emission in the solid state. The other materials show much higher photoluminescence quantum yield in the blend than in the neat film. Whereas **2a** was found to show the highest photoluminescence quantum yield in DCM, the brightest complex in the solid state is **2b**, with a Φ_{PL} in the doped film of 36%, more than double that of **2a**. The emission maxima found in the doped films match those observed in dilute DCM solution.

Theoretical calculations

The geometries and electronic structures of complexes **1a** and **2a**, as representative examples of the series, were modelled within Gaussian 09[27] using density functional theory (DFT) and time-dependent DFT (TDDFT).[28] These complexes were modelled using the B3LYP[29] level of theory with the SBKJC-DVZ[30] basis set for iridium, 6-31G* for heavy atoms directly coordinated to iridium and 3-21G* for all other atoms[30a,31] in the presence of the solvent DCM.[32] This methodology has been successfully used by us for other dinuclear iridium complexes.[33] The calculated ground-state geometries well reproduce those found in the crystal structures with the exception of the Ir–Cl bonds, is *ca.* 0.1 Å longer than the experimental value. The resulting Ir···Ir distance of 3.95 Å is thus also overestimated.

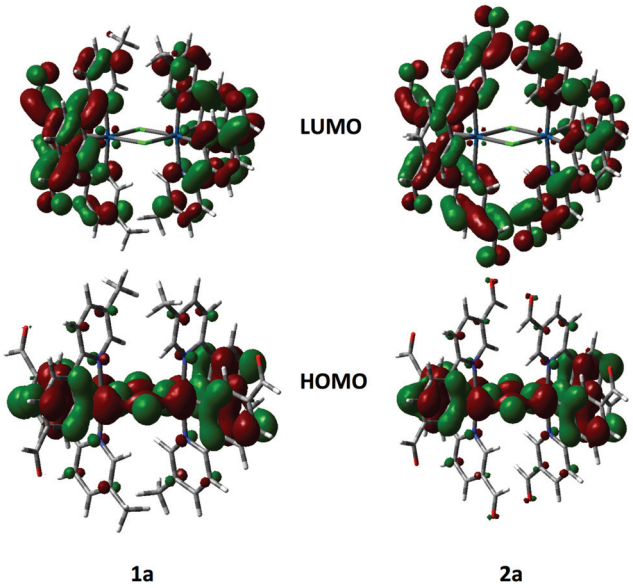

Fig. 8 HOMO and LUMO orbitals of **1a** and **2a**, electron density contour plots at 0.002 e bohr^{-3}.

The frontier molecular orbitals for **1a** and **2b** are shown in Fig. 8. The calculated HOMO and LUMO energies for **1a** are, respectively, −5.59 and −2.20 eV while for **2a** they are −5.90 and −2.90 eV, respectively. Calculated HOMO energies agree very well with CV data in Table 1 while LUMO levels are not well reproduced. The poor prediction for **1a** is most likely a function of the underestimation based on extrapolation of the LUMO level from absorption data. In **2a**, the calculated LUMO is 0.34 eV higher than that obtained from the electrochemical measurement. In both complexes the HOMO is distributed across the iridium dimer with electron density on the iridium metal centers, the phenyl rings of the cyclometalating ligands and the chlorine bridge. This picture, pointing to electronic communication between the two iridium atoms, agrees well with the CV traces, which show two distinct oxidation waves, one at each iridium center. The LUMO is distributed across all of the cyclometalating ligands. In **2a** electron density extends out to the formyl groups on the pyridine rings, which corroborates the assignment of the irreversible reduction in **2a** as being localized on this fragment of the complex. The topologies for HOMO−1 and LUMO+1 are nearly identical to those of HOMO and LUMO, respectively.

The predicted absorption data (Fig. S27 and S28†) obtained by TDDFT reproduce very well the gross features of the absorption spectra, including the low energy band at 540 nm observed in **2a**. The calculated S_0 to T_1 transition obtained from TDDFT based on the S_0 optimized geometries for **1a** and **2a** are 516 and 570 nm fit well with the very weak ^{3}CT transitions observed in the absorption spectra.

Electroluminescence performances

In order to investigate the electrical and optical properties of the OLEDs based on these four iridium dimer complexes, we

tested each of them in a device structure which was ITO/PEDOT:PSS(30 nm)/PVK(30 nm)/CBP : PBD : dimer complex (60 : 30 : 10, 60 nm)/B3PYMPM(40 nm)/Ca(20 nm)/Al(100 nm). PEDOT:PSS, PVK and B3PYMPM denote poly(3,4-ethylenedioxythiophene): poly(styrenesulfonate), poly(*N*-vinylcarbazole) and bis-4,6-(3,5-di-3-pyridylphenyl)-2-methylpyrimidine, respectively. PVK facilitates hole injection because its HOMO (5.6 eV)[34] lies between that of ITO and the co-host materials (6.0 eV). The LUMO of PVK (2.2 eV) is slightly higher than those of CBP (2.6 eV)[35] and PBD (2.3 eV) and its wide energy gap should confine excitons inside the emitting layer thus improving capture of opposite charges in the device.[34,35] The electron-transporting layer B3PYMPM blocks the hole from penetration into the cathode due to its deep-lying HOMO (6.8 eV) and reduces the leakage current.[36] Hence, the multi-layer helps to confine excitons inside the emitting layer as is needed for good luminous efficacy.

Fig. 9 shows the current–voltage characteristics of the devices. The devices with complexes **2a** and **2b** exhibited lower current density at high voltage (>7 V) than the devices made from **1a** and **1b**. The device based on **1b** exhibited the highest current density above 7 V. However, its luminance saturated at higher driving voltage. The devices based on complex **2b** possessed the lowest current density above 7 V. However the luminance of this device goes up very steadily once turned on. A high luminance, up to 5930 cd m^{-2} can be achieved at a driving voltage of 14.6 V. Therefore, among the four complexes, much higher luminous efficiencies can be seen from this device, *i.e.* 9.1 cd A^{-1}, 2.2 lm W^{-1} and 2.6% of current efficiency (CE), power efficiency (PE) and external quantum efficiency (EQE), respectively (Fig. 10a–c, respectively). In contrast, the poorer efficiencies of the devices with **1a** and **1b** may be due to incomplete host to guest energy transfer (**1a**) and exciplex emission (**1b**), which can be inferred from the EL spectra in Fig. 11a and c. The EL spectra from the complexes **2a** and **2b**, were nearly independent of the current density, indicating very efficient host to guest energy transfer and nearly no exciplex contribution (Fig. 11b and d). A comparison of the electrical and optical properties is listed in Table 4.

There is a correlation between the EQE of our devices and solid-state photoluminescence quantum yield (Table 3). The

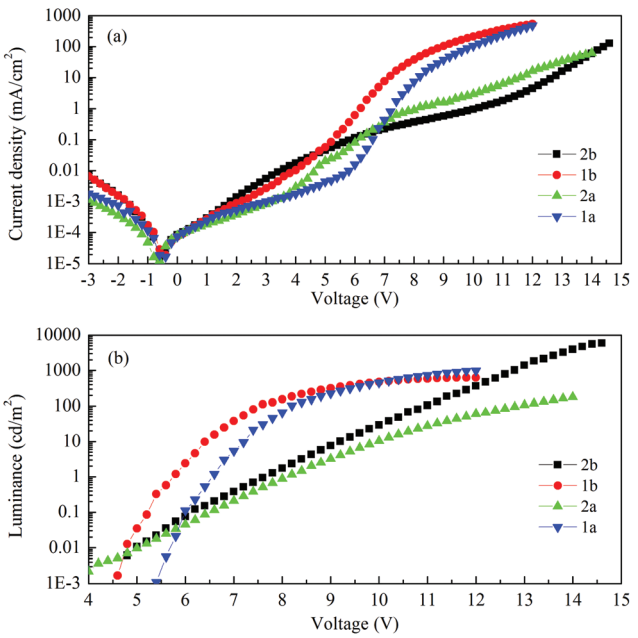

Fig. 9 (a) Current density and (b) luminance *vs.* voltage characteristics of the devices.

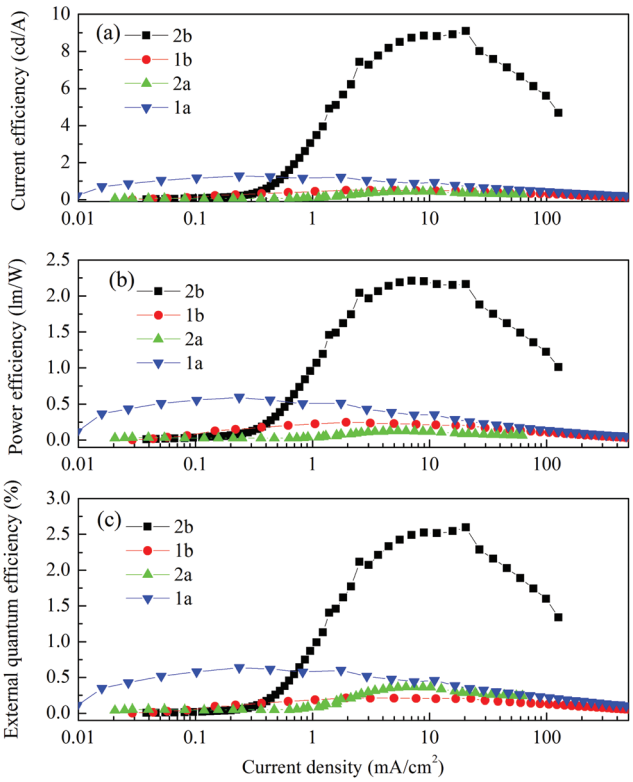

Fig. 10 (a) Current efficiency, (b) power efficiency and (c) external quantum efficiency *vs.* current density characteristics of the devices.

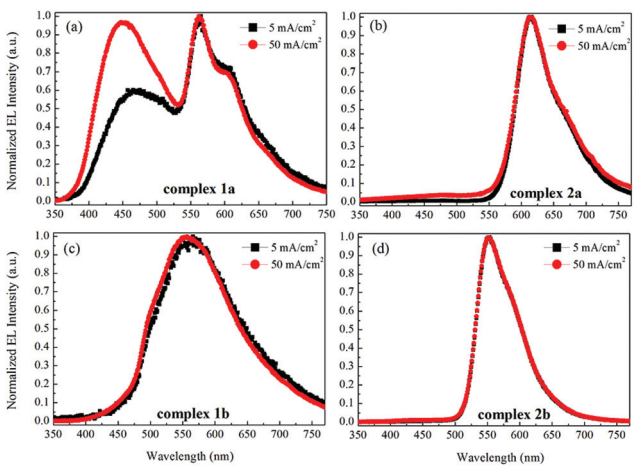

Fig. 11 The normalized EL spectra of the devices with the emitters **1a** (a), **2a** (b), **1b** (c) and **2b** (d) at current densities of 5 and 50 mA cm^{-2}.

Table 4 Comparison of the EL performance of the devices[a]

	Voltage at 1 cd m^{-2} (V)	Max. luminance (cd m^{-2})	Max. CE (cd A^{-1})	Max. PE (lm W^{-1})	Max. EQE (%)	λ_{em} (nm)	CIE at 50 mA cm^{-2}
1a	6.5	982	1.29	0.59	0.64@3 cd m^{-2}	447, 562	(0.3074, 0.3097)
1b	5.7	630	0.51	0.25	0.21@10 cd m^{-2}	612	(0.4073, 0.4966)
2a	8.1	178	0.44	0.13	0.37@28 cd m^{-2}	557	(0.5991, 0.3600)
2b	7.7	>6000	9.09	2.16	2.59@1860 cd m^{-2}	551	(0.4413, 0.5420)

[a] CE = current efficiency. PE = power efficiency. EQE = external quantum efficiency. CIE = The Commission Internationale de l'Eclairage coordinates.

material with the highest Φ_{PL} (**2b**) also produces the OLED with the highest EQE. The complex with the lowest EQE (**1b**) results from its very poor emission with the lowest Φ_{PL} among the four materials. The other two materials (**1a**, **2a**) have intermediate photoluminescence and electroluminescence efficiencies. Of these two materials, **2a** has higher Φ_{PL} but lower external quantum efficiency in the OLED, suggesting that there is a difference in charge balance between the devices.[37] We observe EL from **1b** even though its PL is very weak. However, the spectrum of the EL (Fig. 11c), suggests it is due to the formation of an exciplex between CBP and B3PYMPM.

In the recent report by Bryce and Monkman on the use of dichloro-bridged iridium dimers as emitters in OLEDs, the devices [structure: ITO/PEDOT:PSS/PVK–PBD (40%)–complex (5%)/Ba/Al] achieved peak EQEs ranging from 0.6–4% with PE ranging from 0.40–3.53 lm W^{-1} and CE of 1.7–12 cd A^{-1} based on complexes that showed Φ_{PL} of 21–41% in chlorobenzene solution.[6b] From Table 4, we can see that **2b** exhibits the best performance of the series and shows comparable metrics to the best dichloro-bridged iridium complex reported by Bryce and Monkman.

Conclusions

In this work, the systematic synthesis, structural and optoelectronic characterization, and electroluminescent device data of a series of four dichloro-bridged iridium dimers with formyl-substituted 2-phenylpyridine C^N ligands were presented. The optoelectronic properties were found to be strongly affected by the number of formyl groups and their regiochemistry. In particular, complex **2a** showed a remarkable photoluminescence quantum yield of 15.7% in DCM solution despite being the reddest emitting complex in the series. In the solid state, be it in a pristine thin film or as a dopant, complex **2b** was found to be the brightest. Of the electroluminescent devices fabricated using these iridium dimers, only the OLED employing **2b** as the emissive dopant gave reasonable device performance, with an EQE of 2.6%.

Experimental section

General synthetic procedures

All the chemicals and reagent grade solvents were purchased and used as received. $Pd(PPh_3)_4$ was synthesized according to the literature.[38] All reactions were performed under a nitrogen atmosphere using Schlenk techniques. Flash column chromatography was carried out using silica gel (Silica-P from Silicycle, 60 Å, 40–63 μm). Analytical thin-layer-chromatography (TLC) was performed with silica plates with aluminum backings (250 μm with F-254 indicator). TLC visualization was accomplished by 254/365 nm UV lamp. ^1H and ^{13}C NMR spectra were recorded on a Bruker Avance spectrometer at 500 MHz and 126 MHz, respectively. For multiplicity assignment in NMR spectra reporting, "s" stands for singlet, "d" for doublet, "t" for triplet, "m" for multiplet and "br" for broad peaks. Deuterated chloroform and methylene chloride were used for NMR spectra recording. Melting points (Mp) were measured using open-ended capillaries on an Electrothermal melting point apparatus and are uncorrected. High-resolution mass spectrometry (HRMS) was performed by EPSRC National Mass Spectrometry Service Centre (NMSSC), Swansea. Gas chromatography-mass spectrometry (GC-MS) was recorded on Hewlett Packward HP6890 series GC system tandem with 5973 Mass Selective Detector.

Ligand syntheses

2-Bromo-5-formylpyridine. The synthesis was adapted from methods previously reported.[38,39] Thus, to a suspension of 2,5-dibromopyridine (5.0 g, 21.1 mmol, 1 equiv.) in diethyl ether (50 mL) at −78 °C was added dropwise 1.6 M *n*-butyllithium in hexanes (16 mL, 25.6 mmol, 1.2 equiv.). The reaction mixture was allowed to stir for 30 minutes at this temperature and a dark crimson suspension was observed. Dry DMF (6 mL, 77.8 mmol, 3.5 equiv.) was added and the reaction mixture was allowed to warm to room temperature and stirred for a further 30 minutes. The reaction mixture was then poured into 10% HCl (80 mL) and allowed to stir for 30 minutes. The mixture was then made mildly basic (*ca.* pH = 9.5) with sat. $NaHCO_3$ (aq.). The mixture was extracted with DCM (3 × 50 mL). The combined organic layer was dried with anhydrous Na_2SO_4 and concentrated under reduced pressure. The crude at this stage contained largely pure product according to TLC. Recrystallization from DCM–hexanes afforded the title compound.

Light tan solid. **Yield**: 63%. R_f: 0.41 (EtOAc–Hexanes = 1 : 3 on silica). **Mp**: 100–101 °C (Lit. 100–101 °C).[40] **^1H NMR (300 MHz, $CDCl_3$) δ (ppm)**: 10.09 (s, 1 H), 8.82 (dd, J = 2.4, 0.7 Hz, 1 H), 8.02 (dd, J = 8.2, 2.4 Hz, 1 H), 7.68 (dt, J = 8.2, 0.7 Hz, 1 H). **^{13}C NMR (76 MHz, $CDCl_3$) δ (ppm)**: 189.8, 152.9, 148.7, 137.9, 131.0, 129.4. **GC-MS**: 13.2 min, *m*/*z*: 185 (M), 184 (M − H), 156 (M − CHO).

General procedure for Suzuki–Miyaura cross-coupling

The appropriate 2-bromopyridine (1.0 equiv.) and arylboronic acid (1.1 equiv.), sodium carbonate (3.3 equiv.) and tetrakis-(triphenylphosphine)palladium(0) (5 mol%) were mixed in dioxane–water (4 : 1 v/v, 30 mL per 1 g bromopyridine). The mixture was degassed by freeze–pump–thaw for three cycles. It was then allowed to heat under N_2 at 90 °C for 8 h. The mixture was cooled to room temperature and extracted with DCM (3×). The combined organic phase was dried with anhydrous Na_2SO_4 and concentrated under reduced pressure. The residue was purified by flash column chromatography (silica, hexanes–EtOAc–triethylamine = 80 : 17 : 3) to offer the corresponding ligand.

2-(4-Formylphenyl)-5-methylpyridine (4-CHOmppy). White solid. **Yield**: 92%. R_f: 0.32 (EtOAC–Hexanes = 1 : 3 on silica). **Mp**: 83–84 °C. **^{1}H NMR (300 MHz, $CDCl_3$) δ (ppm):** 10.02 (s, 1 H), 8.51–8.52 (m, 1 H), 8.10 (dt, J = 8.3, 1.6 Hz, 2 H), 7.92 (dt, J = 8.6, 1.7 Hz, 2 H), 7.65 (d, J = 7.6 Hz, 1 H), 7.55 (ddd, J = 8.1, 2.3, 0.7 Hz, 1 H), 2.35 (s, 3 H). **^{13}C NMR (76 MHz, $CDCl_3$) δ (ppm):** 192.3, 153.5, 150.8, 145.3, 137.9, 136.5, 133.3, 130.5, 127.6, 121.0, 18.6. **HR-MS**(ASAP): **$[M + H]^+$ Calculated: ($C_{13}H_{11}NO$)** 198.0913; **Found** 198.0913.

2-(4-Formylphenyl)-5-formylpyridine (4-CHOfppy). White solid. **Yield**: 86%. R_f: 0.22 (EtOAC–Hexanes = 1 : 3 on silica). **Mp**: 158–159 °C. **^{1}H NMR (300 MHz, $CDCl_3$) δ (ppm)**: 10.18 (s, 1 H), 10.12 (s, 1 H), 9.18 (dd, J = 2.2, 0.8 Hz, 1 H), 8.31–8.25 (m, 3 H), 8.05–8.02 (m, 2 H), 7.99 (dt, J = 8.2, 0.7 Hz, 1 H). **^{13}C NMR (76 MHz, $CDCl_3$) δ (ppm)**: 192.1, 190.6, 160.9, 152.7, 143.7, 137.7, 137.3, 130.9, 130.6, 128.6, 121.7. **HR-MS** (ASAP): **$[M + H]^+$ Calculated: ($C_{13}H_9NO_2$)** 212.0706; **Found** 212.0706.

2-(3-Formylphenyl)-5-methylpyridine (3-CHOmppy). Colorless oil. **Yield**: 91%. R_f: 0.35 (EtOAC–Hexanes = 1 : 3 on silica).**^{1}H NMR (300 MHz, $CDCl_3$) δ (ppm)**: 10.10 (s, 1 H), 8.54–8.53 (m, 1 H), 8.47 (td, J = 1.7, 0.6 Hz, 1 H), 8.26 (ddd, J = 7.8, 1.9, 1.2 Hz, 1 H), 7.90 (dt, J = 7.7, 1.4 Hz, 1 H), 7.69 (dd, J = 8.1, 0.9 Hz, 1 H), 7.64–7.57 (m, 2 H), 2.38 (s, 3 H). **^{13}C NMR (76 MHz, $CDCl_3$) δ (ppm)**: 192.8, 153.6, 150.7, 140.6, 138.0, 137.3, 132.9, 129.9, 129.8, 128.6, 120.5, 18.6. **HR-MS** (ASAP): **$[M + H]^+$ Calculated: ($C_{13}H_{11}NO$)** 198.0913; **Found** 198.0913.

2-(3-Formylphenyl)-5-formylpyridine (3-CHOfppy). White solid. **Yield**: 87%. R_f: 0.23 (EtOAC–Hexanes = 1 : 3 on silica). **Mp**: 123–124 °C. **^{1}H NMR (300 MHz, $CDCl_3$) δ (ppm)**: 10.17 (s, 1 H), 10.14 (s, 1 H), 9.17 (dd, J = 2.2, 0.9 Hz, 1 H), 8.60 (td, J = 1.9, 0.5, 1 H), 8.39 (ddd, J = 7.8, 2.0, 1.2 Hz, 1 H), 8.29 (dd, J = 8.3, 2.2 Hz, 1 H), 8.03–7.98 (m, 2 H), 7.70 (t, J = 8.4 Hz, 1 H). **^{13}C NMR (76 MHz, $CDCl_3$) δ (ppm)**: 192.3, 190.7, 160.9, 152.8, 139.3, 137.4, 137.3, 133.6, 131.6, 130.7, 130.2, 129.2, 121.1. **HR-MS** (ASAP): **$[M + H]^+$ Calculated: ($C_{13}H_9NO_2$)** 212.0706; **Found** 212.0706.

General procedure for the synthesis of chloro-bridged iridium dimer complexes $[Ir(C\hat{}N)_2Cl]_2$

Iridium trichloride trihydrate (1 equiv.) and the appropriate C^N ligand (2.2 equiv.) were mixed in 2-alkoxyethanol–water (v/v = 3 : 1, 8 mL for 100 mg $IrCl_3{\cdot}H_2O$). 2-Ethoxyethanol was used for the *mppy* series while 2-methoxyethanol for the *fppy* series. The mixture was degassed *via* three freeze–pump–thaw cycles and was allowed to reflux for 18 h under N_2. After cooling, the precipitate was filtered followed by washing with ethanol and acetone to afford the corresponding $[Ir(C\hat{}N)_2Cl]_2$ complex.

Tetrakis[2-(4′-formylpheny)-5-methylpyridine-C^2,N']-bis-(μ-chloro)diiridium(III) $[Ir(4\text{-}CHOmppy)_2Cl]_2$, 1a. Orange solid. **Yield**: 58%. R_f: 0.55 (DCM–EA = 1 : 1 on silica). **Mp**: not observed below 400 °C. Elemental Analysis (%); Cacld. (found): C 50.36 (50.51); H 3.25 (3.22); N 4.52 (4.58). **^{1}H NMR (400 MHz, CD_2Cl_2) δ (ppm):** 9.42 (s, 4 H), 9.07 (s, 4 H), 7.92 (d, J = 8.3 Hz, 4 H), 7.76 (dd, J = 8.4, 0.8 Hz, 4 H), 7.61 (d, J = 8.0 Hz, 4 H), 7.23 (dd, J = 8.0, 1.6 Hz, 4 H), 6.16 (d, J = 1.6 Hz, 4 H), 2.03 (s, 12 H). **^{13}C NMR (100 MHz, CD_2Cl_2) δ (ppm)**: 192.2, 164.2, 151.9, 150.2, 143.7, 138.5, 135.7, 133.7, 131.6, 123.6, 122.9, 119.9, 18.5. **HR-MS (ESI): M^+ Calculated: ($C_{52}H_{40}Cl_2Ir_2N_4O_4$)** 1240.2; **Found** 1240.1.

Tetrakis[2-(3′-formylpheny)-5-methylpyridine-C^2,N']-bis-(μ-chloro)diiridium(III) $[Ir(3\text{-}CHOmppy)_2Cl]_2$, 1b. Yellow solid. **Yield**: 61%. R_f: 0.41 (DCM–EA = 1 : 1 on silica). **Mp**: 386 °C (decompose). Elemental Analysis (%); Cacld. (found): C 50.36 (50.26); H 3.25 (3.17); N 4.52 (4.57). **^{1}H NMR (400 MHz, CD_2Cl_2) δ (ppm)**: 9.81 (s, 4 H), 9.10 (dd, J = 1.4, 0.8 Hz, 4 H), 8.08 (d, J = 8.2 Hz, 4 H), 8.05 (d, J = 1.8 Hz, 4 H), 7.87 (ddd, J = 8.3, 2.0, 0.5 Hz, 4 H), 7.08 (dd, J = 8.0, 1.8 Hz, 4 H), 6.07 (d, J = 8.0 Hz, 4 H), 2.12 (s, 12 H). **^{13}C NMR (100 MHz, CD_2Cl_2) δ (ppm)**: 191.2, 164.3, 156.3, 151.5, 145.2, 138.8, 133.1, 131.4, 130.8, 130.1, 123.2, 119.0, 18.5. **HR-MS (ESI): M^+ Calculated: ($C_{52}H_{40}Cl_2Ir_2N_4O_4$)** 1240.2; **Found** 1240.2.

Tetrakis[2-(4′-formylpheny)-5-formylpyridine-C^2,N']-bis-(μ-chloro)diiridium(III) $[Ir(4\text{-}CHOfppy)_2Cl]_2$, 2a. Deep red solid. **Yield**: 45%. R_f: 0.32 (DCM–EA = 1 : 1 on silica). **Mp**: 374 °C (decompose). Elemental Analysis (%); Cacld. (found): C 48.19 (48.31); H 2.49 (2.29); N 4.32 (4.28). **^{1}H NMR (400 MHz, CD_2Cl_2) δ (ppm)**: 9.74 (dd, J = 1.9, 0.8 Hz, 4 H), 9.67 (s, 4 H), 9.58 (s, 4 H), 8.37–8.31 (m, 8 H), 7.92 (d, J = 8.0 Hz, 4 H), 7.44 (dd, J = 8.1, 1.6 Hz, 4 H), 6.35 (d, J = 1.5 Hz, 4 H). **^{13}C NMR (100 MHz, CD_2Cl_2) δ (ppm):** 191.7, 187.6, 172.0, 153.6, 147.9, 146.3, 137.9, 137.0, 131.6, 131.2, 126.5, 123.6, 120.7. **HR-MS (ESI): M^+ Calculated: ($C_{52}H_{40}Cl_2Ir_2N_4O_4$)** 1296.1; **Found** 1296.1.

Tetrakis[2-(3′-formylpheny)-5-formylpyridine-C^2,N']-bis-(μ-chloro)diiridium(III) $[Ir(3\text{-}CHOfppy)_2Cl]_2$, 2b. Orange solid. **Yield**: 37%. R_f: 0.25 (DCM–EA = 1 : 1 on silica). **Mp**: 337 °C (decompose). Elemental Analysis (%); Cacld. (found): C 48.19 (48.26); H 2.49 (2.60); N 4.32 (4.45). **^{1}H NMR (300 MHz, CD_2Cl_2) δ (ppm):** 9.84 (s, 4 H), 9.64 (s, 8 H), 8.34–8.33 (m, 8 H), 8.21 (d, J = 1.8 Hz, 4 H), 7.17 (dd, J = 8.1, 1.7 Hz, 4 H), 6.13 (d, J = 8.1 Hz, 4 H). **^{13}C NMR (100 MHz, CD_2Cl_2) δ (ppm):** 190.7, 187.5, 172.1, 157.5, 153.4, 143.3, 137.9, 132.1, 131.7, 131.4, 131.0, 126.4, 120.0. **HR-MS (ESI): M^+ Calculated: ($C_{52}H_{40}Cl_2Ir_2N_4O_4$)** 1296.1; **Found** 1296.1.

X-Ray crystallography

Data for complexes **1a**, **1b** and **2a** were collected at 173 K by using a Rigaku FR-X Ultrahigh brilliance Microfocus RA gen-

Table 5 Crystallographic data for **1a–2b**

	1a	1b	2a	2b
Formula	$C_{53}H_{42}Cl_4Ir_2N_4O_4$	$C_{52}H_{40}Cl_2Ir_2N_4O_4$	$C_{54}H_{36}Cl_6Ir_2N_4O_8$	$C_{52}H_{32}Cl_2Ir_2N_4O_8$
M (g mol^{-1})	1410.12	1240.26	1466.06	1296.19
Crystal system	Monoclinic	Monoclinic	Monoclinic	Monoclinic
Space group	$P2_1/c$	$P2_1/c$	$P2_1/n$	$P2_1/c$
a [Å]	11.065(2)	11.0995(19)	22.9927(11)	11.800(3)
b [Å]	37.753(6)	20.038(3)	11.5838(5)	24.431(6)
c [Å]	13.197(3)	29.679(5)	38.7370(18)	19.925(5)
β [°]	114.701(6)	99.998(4)	97.2195(13)	97.874(6)
V [Å^3]	5008.5(17)	6500.7(18)	10 235.5(8)	5690(2)
Z	4	4	8	4
ρ_{calcd} (g cm^{-3})	1.870	1.267	1.903	1.513
μ (mm^{-1})	5.695	4.219	5.583	9.999
Measured refln.	51 348	97 749	152 461	56 622
Unique refln. (R_{int})	9097 (0.0756)	11 956 (0.1210)	18 712 (0.0527)	10 268 (0.1622)
R_1 [$I > 2\sigma(I)$]	0.0487	0.1243	0.0367	0.1313
wR_2 (all)	0.1378	0.3092	0.1034	0.3816

erator/confocal optics and Rigaku XtaLAB P200 system using Mo Kα radiation (λ = 0.71073 Å). Intensity data were collected using ω steps accumulating area detector images spanning at least a hemisphere of reciprocal space. Data for complex **2b** was collected at 173 K by using a Rigaku MM-007HF High brilliance RA generator/confocal optics and Rigaku XtaLAB P100 system, with Cu Kα radiation (λ = 1.54187 Å). Intensity data were collected using ω and φ steps accumulating area detector images spanning at least a hemisphere of reciprocal space. Data for all complexes were corrected for Lorentz polarization effects. A multiscan absorption correction was applied by using CrystalClear.[41] Structures were solved by Patterson methods (PATTY)[42] and refined by full-matrix least-squares against F^2 (SHELXL-2013).[43] Non-hydrogen atoms were refined anisotropically, and hydrogen atoms were refined using a riding model. Complex **2a** showed discrete disorder in one of the formyl groups, which was modelled over two sites. Both complexes **2a** and **2b** showed signs of unresolvable disorder in various of the formyl groups. Restraints to some bond distances, angles and some thermal parameters were required. All calculations were performed using the CrystalStructure interface.[44] Crystallographic data for the four complexes are listed in Table 5. CCDC 1026256–1026259.

Photophysical measurements

Optically dilute solutions of concentrations on the order of 10^{-5} or 10^{-6} M were prepared in HPLC grade DCM for absorption and emission analysis, respectively. Absorption spectra were record at room temperature on a Shimadzu UV-1800 double beam spectrophotometer in a sealed quartz cuvette from Starna. Molar absorptivity values were determined from at least four solutions with concentrations varying from 3.39 × 10^{-6} M to 4.17 × 10^{-5} M followed by linear regression analysis with all results having coefficient of determination (*r*-squared values) being at least 0.998. Solutions were degassed *via* three freeze–pump–thaw cycles prior to emission analysis in a home-built quartz cuvette. Steady state emission, excitation spectra and time-resolved emission spectra were recorded at 298 K using an Edinburgh Instruments F980. Samples were excited at 455 nm for steady state measurements while at 470 nm for time-resolved measurements. Photoluminescence quantum yields were determined using the optically dilute method[45] in which four sample solutions with absorbance values of 0.10, 0.080, 0.060 and 0.040 at 455 nm were used. For each sample, linearity between absorption and emission intensity was verified through linear regression analysis and additional measurements were acquired until the Pearson regression factor (R^2) for the linear fit of the data set surpassed 0.9. Individual relative quantum yield values were calculated for each solution and the values reported represent the slope value. The equation $\Phi_s = \Phi_r(A_r/A_s)(I_s/I_r)(n_s/n_r)^2$ was used to calculate the relative quantum yield of each of the sample, where Φ_r is the absolute quantum yield of the reference, n is the refractive index of the solvent, A is the absorbance at the excitation wavelength, and I is the integrated area under the corrected emission curve. The subscripts s and r refer to the sample and reference, respectively. A solution of $[Ru(bpy)_3](PF_6)_2$ in ACN (Φ_r = 0.095) was used as the external reference.[26]

Electrochemistry measurements

Cyclic Voltammetry (CV) analysis was performed on an Electrochemical Analyzer potentiostat model CH600D from CH Instruments. Samples were prepared as DCM solutions, which were degassed by sparging with DCM-saturated nitrogen gas for 15 min prior to measurements. All measurements were performed in 0.1 M DCM solution of nBu$_4$NPF$_6$, which acted as the supporting electrolyte. An Ag/Ag$^+$ electrode was used as the reference electrode while a platinum electrode and a platinum wire were used as the working electrode and counter electrode, respectively. The redox potentials are reported relative to a standard calomel electrode (SCE) with a ferrocenium/ferrocene (Fc$^+$/Fc) redox couple as an internal reference (0.46 V *vs.* SCE).[18]

Density functional theory (DFT) calculations

All calculations were performed with the Gaussian 09[27] suite. The level of theory for all DFT[28c,46] and TD-DFT[28d–f] calculations was B3LYP; excited-state triplet geometries were calcu-

lated using the unrestricted B3LYP method (UB3LYP).[29b,c,47] The 6-31G* basis set[48] was used for C, H and N directly linked to Iridium while the other C, H, N and F atoms where undertaken with 3-21G* basis set,[30a,31a–e] and the VDZ (valence double ζ) with SBKJC effective core potential basis set[30] was used for Iridium. The predicted phosphorescence wavelengths were obtained by energy difference between the triplet and singlet states at their respective optimized geometries.[49] The energy, oscillator strength and related MO contributions for the 100 lowest singlet–singlet and 5 lowest singlet–triplet excitations were obtained from the TD-DFT/singlets and the TD-DFT/triplets output files, respectively. The calculated absorption spectra were visualized with GaussSum 2.1 (fwhm: 1000 cm^{-1}).[50]

OLED fabrication and characterization

The PEDOT:PSS layer was spin-coated on pre-patterned ITO glass substrate after ultrasonic cleaning in acetone and 2-propanol consecutively and finally oxygen plasma treatment. PVK, serving as a hole transporting layer, was spin-coated directly onto PEDOT:PSS after baking at 120 °C for 10 minutes in the glove-box to remove the residual moisture. After another baking of PVK at 120 °C for 10 minutes, the emitting layer, comprising of the mixture of the iridium dimer complexes (dissolved in DCM) and hosts (dissolved in chlorobenzene), was spin-coated on PVK. An additional electron transporting layer, B3PYMPM, was thermally evaporated onto the active layer. Finally, Ca (20 nm)/Al (100 nm) as the composite cathode was thermally deposited through a shadow mask in the vacuum chamber under a pressure of 2.0×10^{-6} mbar. All the devices were encapsulated with UV epoxy resin in the glove-box. The luminance–current–voltage measurement was conducted in ambient environment by using Keithley 2400 source meter and 2000 multi-meter connected to a calibrated Si photodiode. The external quantum efficiency was calculated with the assumption of a Lambertian distribution. The electroluminescence spectrum was captured by an Andor DV420-BV CCD spectrometer. The layer thickness was measurement using a Veeco DekTak 150 surface profiler.

Notes and references

1 (*a*) H. Yersin, *Highly Efficient OLEDs with Phosphorescent Materials*, Wiley-VCH, Weinheim, 2008; (*b*) M. C. Gather, A. Köhnen and K. Meerholz, *Adv. Mater.*, 2011, **23**, 233; (*c*) *WOLEDs and Organic Photovoltaics: Recent Advances and Applications*, ed. V. W. W. Yam, 2010; (*d*) C. Fan and C. Yang, *Chem. Soc. Rev.*, 2014, **43**, 6439; (*e*) G. M. Farinola and R. Ragni, *Chem. Soc. Rev.*, 2011, **40**, 3467.

2 (*a*) E. A. Plummer, A. van Dijken, J. W. Hofstraat, L. De Cola and K. Brunner, *Adv. Funct. Mater.*, 2005, **15**, 281; (*b*) C. Adachi, M. A. Baldo, M. E. Thompson and S. R. Forrest, *J. Appl. Phys.*, 2001, **90**, 5048; (*c*) S. Lamansky, P. Djurovich, D. Murphy, F. Abdel-Razzaq, H.-E. Lee, C. Adachi, P. E. Burrows, S. R. Forrest and M. E. Thompson, *J. Am. Chem. Soc.*, 2001, **123**, 4304.

3 (*a*) M. A. Baldo, D. F. O'Brien, Y. You, A. Shoustikov, S. Sibley, M. E. Thompson and S. R. Forrest, *Nature*, 1998, **395**, 151; (*b*) H. Yersin, A. F. Rausch, R. Czerwieniec, T. Hofbeck and T. Fischer, *Coord. Chem. Rev.*, 2011, **255**, 2622.

4 Y. Chi and P.-T. Chou, *Chem. Soc. Rev.*, 2010, **39**, 638.

5 (*a*) S. Sprouse, K. A. King, P. J. Spellane and R. J. Watts, *J. Am. Chem. Soc.*, 1984, **106**, 6647; (*b*) G. A. Carlson, P. I. Djurovich and R. J. Watts, *Inorg. Chem.*, 1993, **32**, 4483; (*c*) F. O. Garces, K. A. King and R. J. Watts, *Inorg. Chem.*, 1988, **27**, 3464.

6 (*a*) S. Bettington, M. Tavasli, M. R. Bryce, A. S. Batsanov, A. L. Thompson, H. A. A. Attar, F. B. Dias and A. P. Monkman, *J. Mater. Chem.*, 2006, **16**, 1046; (*b*) A. M'Hamedi, A. S. Batsanov, M. A. Fox, M. R. Bryce, K. Abdullah, H. A. Al-Attar and A. P. Monkman, *J. Mater. Chem.*, 2012, **22**, 13529.

7 S. Lamansky, P. Djurovich, D. Murphy, F. Abdel-Razzaq, R. Kwong, I. Tsyba, M. Bortz, B. Mui, R. Bau and M. E. Thompson, *Inorg. Chem.*, 2001, **40**, 1704.

8 (*a*) T. Hofbeck and H. Yersin, *Inorg. Chem.*, 2010, **49**, 9290; (*b*) T. Sajoto, P. I. Djurovich, A. B. Tamayo, J. Oxgaard, W. A. Goddard and M. E. Thompson, *J. Am. Chem. Soc.*, 2009, **131**, 9813; (*c*) A. Endo, K. Suzuki, T. Yoshihara, S. Tobita, M. Yahiro and C. Adachi, *Chem. Phys. Lett.*, 2008, **460**, 155; (*d*) G. St-Pierre, S. Ladouceur, D. Fortin and E. Zysman-Colman, *Dalton Trans.*, 2011, **40**, 11726.

9 (*a*) E. Holder, V. Marin, M. A. R. Meier and U. S. Schubert, *Macromol. Rapid Commun.*, 2004, **25**, 1491; (*b*) L. R. Alrawashdeh, A. I. Day and L. Wallace, *Dalton Trans.*, 2013, **42**, 16478; (*c*) Y. Ma, S. Liu, H. Yang, Y. Wu, C. Yang, X. Liu, Q. Zhao, H. Wu, J. Liang, F. Li and W. Huang, *J. Mater. Chem.*, 2011, **21**, 18974; (*d*) X. Cao, Y. Wu, K. Liu, X. Yu, B. Wu, H. Wu, Z. Gong and T. Yi, *J. Mater. Chem.*, 2012, **22**, 2650; (*e*) M. Zaarour, V. Guerchais, H. Le Bozec, C. Dragonetti, S. Righetto, D. Roberto, F. De Angelis, S. Fantacci and M. G. Lobello, *Dalton Trans.*, 2013, **42**, 155.

10 (*a*) K. K.-W. Lo, C.-K. Chung and N. Zhu, *Chem. – Eur. J.*, 2003, **9**, 475; (*b*) K. K.-W. Lo, K. Y. Zhang, S.-K. Leung and M.-C. Tang, *Angew. Chem., Int. Ed.*, 2008, **47**, 2213; (*c*) S. K. Leung, K. Y. Kwok, K. Y. Zhang and K. K. Lo, *Inorg. Chem.*, 2010, **49**, 4984.

11 N. Miyaura and A. Suzuki, *Chem. Rev.*, 1995, **95**, 2457.

12 X. Wang, P. Rabbat, P. O'Shea, R. Tillyer, E. J. J. Grabowski and P. J. Reider, *Tetrahedron Lett.*, 2000, **41**, 4335.

13 M. Nonoyama, *Bull. Chem. Soc. Jpn.*, 1974, **47**, 767.

14 E. Holder, V. Marin, A. Alexeev and U. S. Schubert, *J. Polym. Sci., Part A: Polym. Chem.*, 2005, **43**, 2765.

15 D. L. Davies, M. P. Lowe, K. S. Ryder, K. Singh and S. Singh, *Dalton Trans.*, 2011, **40**, 1028.

16 S. Bettington, A. L. Thompson, A. Beeby and A. E. Goeta, *Acta Crystallogr., Sect. E: Struct. Rep. Online*, 2004, **60**, m827.

17 (*a*) L. Norel, M. Rudolph, N. Vanthuyne, J. A. G. Williams, C. Lescop, C. Roussel, J. Autschbach, J. Crassous and R. Réau, *Angew. Chem., Int. Ed.*, 2010, **49**, 99; (*b*) F. O. Garces, K. Dedeian, N. L. Keder and R. J. Watts,

Acta Crystallogr., Sect. C: Cryst. Struct. Commun., 1993, **49**, 1117; (*c*) L.-Q. Chen, C.-L. Yang and J.-G. Qin, *Acta Crystallogr., Sect. C: Cryst. Struct. Commun.*, 2005, **61**, m513; (*d*) E. Mesto, F. Scordari, M. Lacalamita, L. De Cola, R. Ragni and G. M. Farinola, *Acta Crystallogr., Sect. C: Cryst. Struct. Commun.*, 2013, **69**, 480; (*e*) L. Chen, C. Yang, M. Li, J. Qin, J. Gao, H. You and D. Ma, *Cryst. Growth Des.*, 2006, **7**, 39; (*f*) E. Baranoff, H. J. Bolink, E. C. Constable, M. Delgado, D. Haussinger, C. E. Housecroft, M. K. Nazeeruddin, M. Neuburger, E. Orti, G. E. Schneider, D. Tordera, R. M. Walliser and J. A. Zampese, *Dalton Trans.*, 2013, **42**, 1073; (*g*) E. C. Constable, C. D. Ertl, C. E. Housecroft and J. A. Zampese, *Dalton Trans.*, 2014, **43**, 5343; (*h*) C. Xu, H. M. Li, Z. Q. Xiao, Z. Q. Wang, S. F. Tang, B. M. Ji, X. Q. Hao and M. P. Song, *Dalton Trans.*, 2014, **43**, 10235; (*i*) Z.-Q. Wang, C. Xu, X.-M. Dong, Y.-P. Zhang, X.-Q. Hao, J.-F. Gong, M.-P. Song and B.-M. Ji, *Inorg. Chem. Commun.*, 2011, **14**, 316; (*j*) K. A. McGee and K. R. Mann, *Inorg. Chem.*, 2007, **46**, 7800; (*k*) C. Xu, Z.-Q. Wang, X.-M. Dong, X.-Q. Hao, X.-M. Zhao, B.-M. Ji and M.-P. Song, *Inorg. Chim. Acta*, 2011, **373**, 306; (*l*) O. Chepelin, J. Ujma, X. Wu, A. M. Z. Slawin, M. B. Pitak, S. J. Coles, J. Michel, A. C. Jones, P. E. Barran and P. J. Lusby, *J. Am. Chem. Soc.*, 2012, **134**, 19334; (*m*) V. Krisyuk, A. Turgambaeva, J. Lee and S.-W. Rhee, *Transition Met. Chem.*, 2005, **30**, 786.

18 N. G. Connelly and W. E. Geiger, *Chem. Rev.*, 1996, **96**, 877.

19 C. M. Cardona, W. Li, A. E. Kaifer, D. Stockdale and G. C. Bazan, *Adv. Mater.*, 2011, **23**, 2367.

20 J.-L. Bredas, *Mater. Horiz.*, 2014, **1**, 17.

21 E. S. Andreiadis, D. Imbert, J. Pécaut, A. Calborean, I. Ciofini, C. Adamo, R. Demadrille and M. Mazzanti, *Inorg. Chem.*, 2011, **50**, 8197.

22 B. Beyer, C. Ulbricht, D. Escudero, C. Friebe, A. Winter, L. González and U. S. Schubert, *Organometallics*, 2009, **28**, 5478.

23 C. E. Welby, L. Gilmartin, R. R. Marriott, A. Zahid, C. R. Rice, E. A. Gibson and P. I. Elliott, *Dalton Trans.*, 2013, **42**, 13527.

24 A. B. Tamayo, B. D. Alleyne, P. I. Djurovich, S. Lamansky, I. Tsyba, N. N. Ho, R. Bau and M. E. Thompson, *J. Am. Chem. Soc.*, 2003, **125**, 7377.

25 S. Ladouceur, D. Fortin and E. Zysman-Colman, *Inorg. Chem.*, 2011, **50**, 11514.

26 H. Ishida, S. Tobita, Y. Hasegawa, R. Katoh and K. Nozaki, *Coord. Chem. Rev.*, 2010, **254**, 2449.

27 M. J. Frisch, G. W. Trucks, H. B. Schlegel, G. E. Scuseria, M. A. Robb, J. R. Cheeseman, G. Scalmani, V. Barone, B. Mennucci, G. A. Petersson, H. Nakatsuji, M. Caricato, X. Li, H. P. Hratchian, A. F. Izmaylov, J. Bloino, G. Zheng, J. L. Sonnenberg, M. Hada, M. Ehara, K. Toyota, R. Fukuda, J. Hasegawa, M. Ishida, T. Nakajima, Y. Honda, O. Kitao, H. Nakai, T. Vreven, J. A. Montgomery Jr., J. E. Peralta, F. Ogliaro, M. Bearpark, J. J. Heyd, E. Brothers, K. N. Kudin, V. N. Staroverov, R. Kobayashi, J. Normand, K. Raghavachari, A. Rendell, J. C. Burant, S. S. Iyengar, J. Tomasi, M. Cossi, N. Rega, J. M. Millam, M. Klene, J. E. Knox, J. B. Cross, V. Bakken, C. Adamo, J. Jaramillo, R. Gomperts, R. E. Stratmann, O. Yazyev, A. J. Austin, R. Cammi, C. Pomelli, J. W. Ochterski, R. L. Martin, K. Morokuma, V. G. Zakrzewski, G. A. Voth, P. Salvador, J. J. Dannenberg, S. Dapprich, A. D. Daniels, Ö. Farkas, J. B. Foresman, J. V. Ortiz, J. Cioslowski and D. J. Fox, 7.0 ed., Wallingford, CT, 2009.

28 (*a*) P. Hohenberg and W. Kohn, *Phys. Rev.*, 1964, **136**, B864; (*b*) W. Kohn and L. J. Sham, *Phys. Rev.*, 1965, **140**, A1133; (*c*) *In The Challenge of d and f Electrons*, ed. D. R. Salahub and M. C. Zerner, ACS, Washington, DC, 1989; (*d*) R. E. Stratmann, G. E. Scuseria and M. J. Frisch, *J. Chem. Phys.*, 1998, **109**, 8218; (*e*) R. Bauernschmitt and R. Ahlrichs, *Chem. Phys. Lett.*, 1996, **256**, 454; (*f*) M. E. Casida, C. Jamorski, K. C. Casida and D. R. Salahub, *J. Chem. Phys.*, 1998, **108**, 4439.

29 (*a*) A. D. Becke, *J. Chem. Phys.*, 1993, **98**, 5648; (*b*) C. Lee, W. Yang and R. G. Parr, *Phys. Rev. B: Condens. Matter*, 1988, **37**, 785; (*c*) B. Miehlich, A. Savin, H. Stoll and H. Preuss, *Chem. Phys. Lett.*, 1989, **157**, 200.

30 (*a*) J. S. Binkley, J. A. Pople and W. J. Hehre, *J. Am. Chem. Soc.*, 1980, **102**, 939; (*b*) W. J. Stevens, W. J. Basch and M. Krauss, *J. Chem. Phys.*, 1984, **81**, 6026; (*c*) W. J. Stevens, M. Krauss, H. Basch and P. G. Jasien, *Can. J. Chem.*, 1992, **70**, 612; (*d*) T. R. Cundari and W. J. Stevens, *J. Chem. Phys.*, 1993, **98**, 5555.

31 (*a*) M. S. Gordon, J. S. Binkley, J. A. Pople, W. J. Pietro and W. J. Hehre, *J. Am. Chem. Soc.*, 1982, **104**, 2797; (*b*) W. J. Pietro, M. M. Francl, W. J. Hehre, D. J. Defrees, J. A. Pople and J. S. Binkley, *J. Am. Chem. Soc.*, 1982, **104**, 5039; (*c*) K. D. Dobbs and W. J. Hehre, *J. Comput. Chem.*, 1986, **7**, 359; (*d*) K. D. Dobbs and W. J. Hehre, *J. Comput. Chem.*, 1987, **8**, 861; (*e*) K. D. Dobbs and W. J. Hehre, *J. Comput. Chem.*, 1987, **8**, 880; (*f*) R. Ditchfield, W. J. Hehre and J. A. Pople, *J. Chem. Phys.*, 1971, **54**, 724; (*g*) W. J. Hehre, R. Ditchfield and J. A. Pople, *J. Chem. Phys.*, 1972, **56**, 2257; (*h*) P. C. Hariharan and J. A. Pople, *Theor. Chim. Acta*, 1973, **28**, 213; (*i*) P. C. Hariharan and J. A. Pople, *Mol. Phys.*, 1974, **27**, 209; (*j*) M. S. Gordon, *Chem. Phys. Lett.*, 1980, **76**, 163.

32 J. Tomasi, B. Mennucci and R. Cammi, *Chem. Rev.*, 2005, **105**, 2999.

33 (*a*) L. Donato, C. E. McCusker, F. N. Castellano and E. Zysman-Colman, *Inorg. Chem.*, 2013, **52**, 8495; (*b*) A. M. Soliman, D. Fortin, P. D. Harvey and E. Zysman-Colman, *Dalton Trans.*, 2012, **41**, 9382.

34 X. H. Yang, F. Jaiser, B. Stiller, D. Neher, F. Galbrecht and U. Scherf, *Adv. Funct. Mater.*, 2006, **16**, 2156.

35 J. Kalinowski, M. Cocchi, D. Virgili, V. Fattori and J. A. G. Williams, *Adv. Mater.*, 2007, **19**, 4000.

36 S. Lee, K.-H. Kim, D. Limbach, Y.-S. Park and J.-J. Kim, *Adv. Funct. Mater.*, 2013, **23**, 4105.

37 C. Adachi, M. A. Baldo, M. E. Thompson and S. R. Forrest, *J. Appl. Phys.*, 2001, **90**, 5048.

38 D. R. Coulson, L. C. Satek and S. O. Grim, in *Inorg. Synth*, ed. F. A. Cotton, 2007, p. 121.
39 A. Bouillon, J.-C. Lancelot, V. Collot, P. R. Bovy and S. Rault, *Tetrahedron*, 2002, **58**, 2885.
40 P. H. Bernardo, T. Sivaraman, K. F. Wan, J. Xu, J. Krishnamoorthy, C. M. Song, L. Tian, J. S. Chin, D. S. Lim, H. Y. Mok, V. C. Yu, J. C. Tong and C. L. Chai, *J. Med. Chem.*, 2010, **53**, 2314.
41 *CrystalClear-SM Expert v. 2.1*, The Woodlands, Texas, USA, 2010–2014.
42 P. T. Beurskens, G. Beurskens, R. de Gelder, S. Garcia-Granda, R. O. Gould, R. Israel and J. M. M. Smits, *DIRDIF-99*, University of Nijmegen, The Netherlands, 1999.
43 G. Sheldrick, *Acta Crystallogr., Sect. A: Fundam. Crystallogr.*, 2008, **64**, 112.
44 *CrystalStructure v4.1*, The Woodlands, Texas, USA, 2014.
45 (*a*) G. A. Crosby and J. N. Demas, *J. Phys. Chem.*, 1971, **75**, 991; (*b*) S. Fery-Forgues and D. Lavabre, *J. Chem. Educ.*, 1999, **76**, 1260.
46 (*a*) P. Hohenberg and W. Kohn, *Phys. Rev.*, 1964, **B136**, 864; (*b*) W. Kohn and L. J. Sham, *Phys. Rev.*, 1965, **A140**, 1133; (*c*) R. G. Parr and W. Yang, *Density-functional theory of atoms and molecules*, Oxford Univ. Press, Oxford, 1989.
47 A. D. Becke, *J. Chem. Phys.*, 1993, **98**, 5648.
48 V. A. Rassolov, J. A. Pople, M. A. Ratner and T. L. Windus, *J. Chem. Phys.*, 1998, **109**, 1223.
49 (*a*) S. Ladouceur, D. Fortin and E. Zysman-Colman, *Inorg. Chem.*, 2010, **49**, 5625; (*b*) M. S. Lowry, W. R. Hudson, R. A. Pascal Jr. and S. Bernhard, *J. Am. Chem. Soc.*, 2004, **126**, 14129.
50 N. M. O'Boyle, *GaussSum 2.0*, Dublin City University, Dubin Ireland, 2006, Available at http://gausssum.sf.net.